This is a preprint, the final version is subject to change, of the American Mineralogist (MSA)
Cite as Authors (Year) Title. American Mineralogist, in press.
DOI: https://doi.org/10.2138/am-2019-6948

1 **Revision 1**

2 Melting temperature depression due to electronic spin transition of iron

3 **Authors:** Jie Deng* and Kanani K. M. Lee

4 **Affiliations:**

5 Department of Geology and Geophysics, Yale University, New Haven CT 06511

6 *Corresponding author.

7 E-mail: jie.deng@yale.edu

8 **Keywords:** melting; spin transition; ferropericlase; bridgmanite; lower mantle

9

This is a preprint, the final version is subject to change, of the American Mineralogist (MSA)
Cite as Authors (Year) Title. American Mineralogist, in press.
DOI: https://doi.org/10.2138/am-2019-6948

Abstract

The electronic spin transition of iron has been shown to strongly affect many physical properties of the host mineral. However, the response of melting temperatures to the spin transition remains largely unexplored. Here, we study the melting of lower mantle minerals, ferropericlase and bridgmanite, using Lindemann's Law. This empirical law predicts a negligible melting temperature depression for Earth-relevant bridgmanite but a substantial depression for Earth-relevant ferropericlase across the spin transition of iron, consistent with extant experimental results. This melting depression can be explained within the framework of Lindemann's Law for a Debye-like solid. The transition of iron from high to low spin configuration reduces the molar volume and the bulk modulus of the crystal, leading to a decrease in Debye frequency and consequently lowering the melting temperature. Thermodynamically, the melting depression likely derives from a more negative Margules parameter for a liquid mixture of high- and low-spin endmembers as compared to that of a solid mixture. This melting depression across the spin transition of iron may be the process responsible for the formation of a deep molten layer during the crystallization of a magma ocean in the past, and a reduced viscosity layer at present.

This is a preprint, the final version is subject to change, of the American Mineralogist (MSA)
Cite as Authors (Year) Title. American Mineralogist, in press.
DOI: https://doi.org/10.2138/am-2019-6948

Introduction

Many minerals in Earth's mantle are believed to contain both ferrous and/or ferric iron. Specifically, for the lower mantle, the iron content of the two major constituents, $(Mg,Fe)SiO_3$ bridgmanite and (Mg,Fe)O ferropericlase are estimated to be 4-10 atomic% and 20-30 atomic%, respectively (Lee et al., 2004; Muir and Brodholt, 2016). Both Fe^{2+} and Fe^{3+} are characterized by the partially-filled 3*d* electron shells and thus multiple electronic spin states. The ionic radii and magnetic moments of iron ions with different electronic configurations in the same crystallographic site are intrinsically distinct. As such, the spin transition of iron is expected to affect the properties of lower mantle minerals. Indeed, recent experiments and first-principles simulations confirm that the spin transition of iron could result in substantial changes in physical (i.e., density and bulk modulus) (Tsuchiya et al., 2006; Crowhurst et al., 2008; Wentzcovitch et al., 2009; Liu et al., 2018), transport (i.e., diffusivity, viscosity, electrical/thermal conductivity) (Ohta et al., 2007; Saha et al., 2011), and chemical (e.g., element partitioning) properties of minerals (Badro et al., 2003; Shim et al., 2017).

Nevertheless, the effect of spin transitions on melting temperature, a fundamental thermodynamic property, remains poorly constrained. Intuitively, anomalous melting behavior is anticipated for a spin-crossover system like (Mg,Fe)O. This is because melting is essentially governed by the energetics of the solid and liquid phases that have been shown to strongly depend on the spin state of the system (Wentzcovitch et al., 2009; Holmström and Stixrude, 2015; Ghosh and Karki, 2016).

Recently, Deng and Lee (2017) observed a pronounced melting temperature depression of ferropericlase of Earth-relevant compositions at pressures greater than ~40

GPa where the spin transition of Fe^{2+} occurs, creating local minima in the solidus and liquidus fusion curves. To our knowledge, this is the first time the effects of spin transition on melting have been proposed.

In order to further explore the effects of the spin transition on the melting temperature, we utilize the semi-empirical Lindemann's Law which states that melting occurs if the mean square amplitude of atomic vibrations exceeds a critical fraction *f* of the interatomic distance in the crystal (Lindemann, 1910; Gilvarry, 1956b). As the properties of the liquid states are not explicitly considered, Lindemann's Law lacks a legitimate physical basis as pointed out by many studies (e.g., Wolf and Jeanloz, 1984; Wallace, 1991). However, the applicability of the Lindemann's Law has been well tested for many systems and some general trends have emerged. Lawson (2009) demonstrated that Lindemann's Law follows from straightforward thermodynamic considerations for elements of simple structure, although it does fail for others with more complicated structures (Wolf and Jeanloz, 1984). Anderson (1995) concluded that Lindemann's Law is applicable to densely packed (i.e., packing fraction is large) Debye-like solids for which a single value of Debye temperature would suffice to describe the thermoelastic properties. For example, MgO, FeO and $MgSiO_3$ bridgmanite are typical Debye-like solids (Anderson, 1998) and the predicted melting curves based on Lindemann's Law exhibit good agreement with the experiments and first-principles computations (Poirier, 1989; Speziale et al., 2001; Fischer and Campbell, 2010). In addition, bridgmanite with 10 atomic% iron is also characterized by Debye-like thermoelastic properties (Anderson and Hama, 1999). Similarly, the (Mg,Fe)O solid solution may also be a Debye-like solid given its two Debye-like endmembers (Anderson, 1995). As a result, Lindemann's Law is likely applicable to

ferropericlase and bridgmanite of Earth-relevant compositions before the spin crossover. Upon the spin transition, components with different spin states are admixed, modifying the atomic vibrations and free energies of the systems. Thus, it is uncertain whether Lindemann's Law would still apply.

In this study, we first investigate the fusion curves of iron-bearing ferropericlase using Lindemann's Law and compare with experimental results. We focus on the spin-transition pressure range and examine whether Lindemann's Law provides a satisfying prediction of the melting curve response to the spin crossover. This analysis allows us to generalize the effects of spin transitions of iron on melting temperatures. Finally, we analyze the thermodynamic meaning of melting depression and compare with other spin-transition induced thermoelastic anomalies.

Lindemann's Law

For a Debye-like solid, Lindemann's Law may be expressed as (Gilvarry, 1956a; Gilvarry, 1956b),

$$T_m = Cf^2V^{2/3}\Theta_D^2 \quad , \qquad (1)$$

where T_{m} is the melting temperature; Θ_D and V are the Debye temperature and molar volume respectively at fusion; f is the critical fraction of the mean square amplitude of atomic vibrations; C is a constant for a given system. Θ_D of the solid at melting is given by

$$\Theta_D = C'SK_T^{1/2}V^{1/6} \quad , \qquad (2)$$

where K_T is the isothermal bulk modulus at melting; S is a function of Poisson's ratio and can be approximated as a constant for the Debye-like solids (Gilvarry, 1956b); C' is a constant for a given system.

Combining the above two equations yields the differential Lindemann equation (Gilvarry, 1956b),

$$\frac{d\ln T_m}{dP} = \frac{1}{K_T}\left(\frac{dK_T}{dP} - 1\right), \quad (3)$$

where P is pressure. From this equation, we can infer that the melting slope is 0 if K_T' (= $\frac{dK_T}{dP}$) is equal to 1.

We choose the differential Lindemann equation in this study to estimate the melting curves for (Mg,Fe)O and (Mg,Fe)SiO_3. This is because while solid ferropericlase and bridgmanite appear to have a nearly constant K_T' ($=\frac{dK_T}{dP}$) at pure high or pure low spin state, K_T' changes dramatically in the pressure range of the spin transition where the spin state is mixed (Crowhurst et al., 2008; Marquardt et al., 2009a; Wentzcovitch et al., 2009; Catalli et al., 2010; Hsu et al., 2011) and therefore should be treated as a free variable. The disadvantage of this treatment is that the evaluation of T_m critically hinges on the scarcity of high temperature (i.e., close to melting temperature) K_T' data.

Melting of (Mg,Fe)O ferropericlase across the spin transition

The spin transition of Fe^{2+} in (Mg,Fe)O ferropericlase is a gradual process and the transition pressure range tends to broaden with increasing temperatures (Lin et al., 2007;

Glazyrin et al., 2016). The thermoelastic properties of (Mg,Fe)O ferropericlase approaching, during and upon completion of the spin-state crossover at room temperature have been extensively studied in the last decade (e.g., Crowhurst et al., 2008; Marquardt et al., 2009a; Marquardt et al., 2009b; Yang et al., 2015; Marquardt et al., 2018). The current agreement is that the spin transition strongly softens the bulk modulus while only marginally affects the shear modulus. Additionally, first-principles computations show that the softening gradually diminishes with increasing temperature (Wentzcovitch et al., 2009).

To our best knowledge, so far the only available bulk modulus data at high temperature (close to melting temperatures) and pressure (across the spin transition pressure) of $(Mg_{1-x}Fe_x)O$ ferropericlase is reported by (Wentzcovitch et al., 2009) for x = 0.1875. It is noted that at some low pressure and high temperature conditions (e.g., T = 3000 K, P< ~50 GPa and T = 4000 K, P< 90 GPa), the quasiharmonic approximation (QHA) is claimed to be invalid (Wentzcovitch et al., 2009). These P-T conditions which lay outside of the QHA are inferred based on thermal expansivity, which is known to be a sensitive parameter to anharmonic effects. In contrast, the bulk modulus is insensitive to the anharmonicity as manifested by the relatively small temperature derivative of bulk modulus (dK_S/dT) for the high-spin (Mg,Fe)O, i.e., ~-0.01-0.02 GPa/K (Yang et al., 2016). Additionally, ferropericlase of (mostly) high-spin state at P-T conditions outside the validity regime of the QHA exhibits similar dK_S/dT (Wentzcovitch et al., 2009). Therefore, we conclude that the valid P-T conditions of the QHA reported by (Wentzcovitch et al., 2009) is only directly relevant to the thermal expansivity. The QHA implemented by (Wentzcovitch et al., 2009) has adequately taken into account the anharmonic effects for bulk modulus even at P-T conditions outside the validity range of the QHA.

Since only the adiabatic bulk modulus (K_S) is provided (Wentzcovitch et al., 2009), we first convert K_S to K_T through $K_T = K_S/(1+\alpha\gamma T)$, where α is the thermal expansion coefficient, and γ is the thermodynamic Grüneisen parameter. As this study focuses on the temperatures close to the melting temperatures (2000-4000 K) and pressures similar to those in experiments by Deng and Lee (2017), we average the α and γ at these P-T conditions reported by Wu et al. (2009) and obtain $\alpha = 2.2\times10^{-5}$ K^{-1} and $\gamma = 1.6$. These values are very close to values determined experimentally (Tange et al., 2009; Mao et al., 2011). The resulting K_T' are plotted in Fig. 1a. For all the temperatures considered here (i.e., 300, 1000, 2000, 3000, 4000 K), K_T' remains mostly constant at ~3.3 before ~25 GPa and then gradually decreases to 1 or smaller values, indicating the existence of local extrema in the melting curve according to Eq. 3.

Three points need clarification before proceeding any further. First, Lindemman's Law is generally used for solidus in the case of incongruent melting since it describes the initiation of melting. Therefore, we only consider the solidus melting temperatures hereafter. Second, in principle K_T and K_T' in Eq. 3 should be evaluated at the melting temperature. In practice, however, we have to use the K_T and K_T' at constant temperatures (i.e., 2000, 3000, 4000 K) because K_T and K_T' at other temperatures are not available (300 K and 1000 K are too cool to be considered relevant here). The solidus melting temperatures of $(Mg_{0.8125}Fe_{0.1875})O$ at pressure < 80 GPa are ~2500-3500 K (Du and Lee, 2014; Deng et al., 2017; Deng and Lee, 2017; Deng et al., 2019), enveloped by the temperatures of available K_T and K_T'. It is expected that the solidus predicted by Lindemann's law using K_T and K_T' at 3000 K will show the best agreement with the experimental solidus. Third, one melting point is required as the anchor point to integrate

159 Eq. 3. Here we choose the solidus melting temperature of 3460 K at 40 GPa as the anchor
160 point as most experiments (Deng and Lee, 2017) have been performed at or near this
161 pressure to constrain the phase diagram.

162 The solidus curves calculated using K_T and K_T' at 2000, 3000 and 4000 K are
163 shown in Fig. 1b. For the melting points at pressures less than 40 GPa, experimental results
164 agree very well with the Lindemann's Law prediction regardless of K_T and K_T' used. At
165 pressures greater than 40 GPa, the agreement is best using K_T and K_T' at 2000 K, which
166 appears too low of a temperature for our expectations that the K_T and K_T' values should be
167 at the temperatures of the solid just prior to melting. A much better agreement between the
168 Lindemann's Law predictions using K_T and K_T' at 3000 K and experiments (Du and Lee,
169 2014; Deng and Lee, 2017) emerges once the thermal pressure (i.e., an additional ~8-13
170 GPa) involved in the experiments (Fiquet et al., 1996) is taken into consideration (Fig. 1c).
171 Additionally, the good agreement between melting curves calculated based on the bulk
172 modulus at 3000 K and thermal pressure-corrected melting points is not strongly affected
173 by the anchor point used (Fig. S1).

174 The solidus melting curve predicted by Lindemann's Law with K_T and K_T' at 3000
175 K shows a substantial depression between ~50-100 GPa and this depression peaks at ~80
176 GPa. The melting temperature is ~700 K lower than that if the melting curve follows the
177 trend of melting curves of either pure high spin (HS) or low spin (LS) (Mg,Fe)O. This
178 depression can be explained as follows. The spin transition of iron from high to low tends
179 to reduce the molar volume of the crystal and significantly soften the bulk modulus, leading
180 to a decrease in Debye temperature (frequency) and consequently lowering the melting
181 temperature according to Eq. 1.

This is a preprint, the final version is subject to change, of the American Mineralogist (MSA)
Cite as Authors (Year) Title. American Mineralogist, in press.
DOI: https://doi.org/10.2138/am-2019-6948

In summary, the melting temperature depression of (Mg,Fe)O across the spin transition observed in the experiments is consistent with the Lindemann's law prediction. The good agreement also validates the application of this semi-empirical law to the solidus of (Mg,Fe)O regardless of the spin crossover. In other words, the spin crossover does not appear to affect the applicability of Lindemann's Law, which may enable us to generalize the effects of the spin transition on the melting temperature.

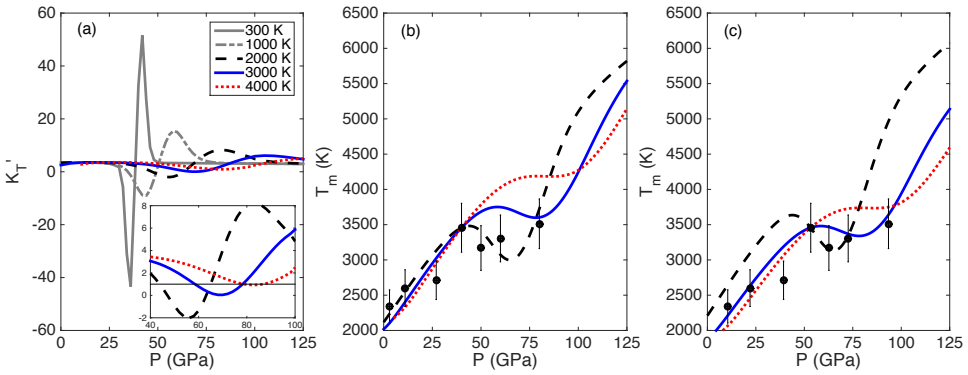

FIGURE 1. Comparison of $(Mg_{0.8125}Fe_{0.1875})O$ ferropericlase melting curves predicted by Lindemann's Law with results based on experimentally-determined phase diagrams (black circles) (Du and Lee, 2014; Deng and Lee, 2017; Deng et al., 2019). **(a)** The evolution of K_T' with pressure across the spin transition at 300 K (grey solid), 1000 K (grey dash-dotted), 2000 K (black dashed), 3000 K (blue solid) and 4000 K (red dotted). The inset panel shows the intersection of K_T' with 1 (horizontal line) for 2000 K, 3000 K, and 4000 K isotherms, corresponding to a melting slope of zero (Eq. 3). **(b)** Solidus curves of (Mg,Fe)O predicted by Lindemann's Law with the anchor point at 40 GPa. The colors represent the calculated bulk moduli at the given temperature used in the melting curve calculations. **(c)** Same as B except the experimental data (pressures initially reported at

199 room temperature) are corrected for thermal pressure expected when exposed to high
200 temperatures (Fiquet et al., 1996).

201

202 **Melting temperature depression for (Mg,Fe)SiO_3 bridgmanite?**

203 (Mg,Fe)(Si,Fe)O_3 bridgmanite has an orthorhombic structure with Fe^{2+} mainly
204 entering the A site (the large 8/12-fold pseudo-dodecahedral site) and Fe^{3+} in both A site
205 and B site (the smaller 6-fold octahedral site) depending on the amount of Al-Si
206 substitution (McCammon, 1997; Kupenko et al., 2015). The coexistence of Fe^{2+} and Fe^{3+}
207 and their complicated occupancy states cause a big challenge for the study of spin
208 transitions in bridgmanite. The current consensus is that A-site Fe^{2+} does not undergo spin
209 transition (e.g., Lin et al., 2013; Lin et al., 2016) while the B-site Fe^{3+} undergoes a HS to
210 LS transition at high pressures, although the transition pressure in previous studies varies
211 [i.e., 42-63 GPa for bridgmanite of Fe_2O_3 content ~10 mol% (Catalli et al., 2010; Hsu et
212 al., 2011; Tsuchiya and Wang, 2013; Lin et al., 2016; Shukla et al., 2016a; Liu et al.,
213 2018)].

214 Similar to (Mg,Fe)O ferropericlase, the spin transition of the B-site Fe^{3+} in
215 (Mg,Fe)(Si,Fe)O_3 bridgmanite is also a smooth transition with wider transition pressure
216 ranges at higher temperatures. The thermoelastic data of Fe^{3+} -bearing bridgmanite at high
217 pressure and temperature as computed using density functional theory are available for
218 $(Mg_{0.875}Fe^{3+}_{0.125})(Si_{0.875}Fe^{3+}_{0.125})O_3$ (Hsu et al., 2011; Shukla and Wentzcovitch, 2016),
219 $(Mg_{0.9375}Fe^{3+}_{0.0625})(Si_{0.9375}Fe^{3+}_{0.0625})O_3$ (Tsuchiya and Wang, 2013), and
220 $(Mg_{0.95}Fe^{3+}_{0.05})(Si_{0.\ 95}Fe^{3+}_{0.05})O_3$ (Shukla et al., 2016a). Experimental studies on the

melting of Fe-bearing bridgmanite are available for $(Mg_{0.9}Fe_{0.1})SiO_3$ (Heinz and Jeanloz, 1987) and $(Mg_{0.88}Fe_{0.12})SiO_3$ (Knittle and Jeanloz, 1989; Zerr and Boehler, 1993). Here we focus on the thermoelastic properties of $(Mg_{0.9375}Fe^{3+}_{0.0625})(Si_{0.9375}Fe^{3+}_{0.0625})O_3$ (Tsuchiya and Wang, 2013) and $(Mg_{0.95}Fe^{3+}_{0.05})(Si_{0.95}Fe^{3+}_{0.05})O_3$ (Shukla et al., 2016a) for a direct comparison.

Following the same protocol as for (Mg,Fe)O, we derive K'_T and integrate Eq. 3 to obtain the melting temperature. Since the melting temperatures of bridgmanite of ~10 mol% iron are above 2000 K (Heinz and Jeanloz, 1987; Knittle and Jeanloz, 1989; Zerr and Boehler, 1993), only the bulk modulus data at temperatures > 2000 K are suitable to calculate the melting temperature using Lindemann's Law. We thus only present the results based on the high temperature bulk modulus data (> 2000 K) (Fig. 2). The reference melting point we choose is 3000 K and 24 GPa (Zerr and Boehler, 1993). For completeness, we also present the analyses of literature results (Hsu et al., 2011; Tsuchiya and Wang, 2013; Shukla et al., 2016b; Shukla and Wentzcovitch, 2016) at lower temperatures in Fig. S2 a-d.

K'_T of $(Mg_{0.9375}Fe^{3+}_{0.0625})(Si_{0.9375}Fe^{3+}_{0.0625})O_3$ at 3000 and 4000 K and $(Mg_{0.95}Fe^{3+}_{0.05})(Si_{0.95}Fe^{3+}_{0.05})O_3$ at 2700 K decrease with pressure and does not show any obvious anomalies as we find with (Mg,Fe)O. This is because spin transition only marginally affects the bulk modulus of bridgmanite of ~10 mol% iron content is negligibly small at these high temperatures (Tsuchiya and Wang, 2013; Shukla et al., 2016a). As such, the spin transition of iron cannot be the main cause of the flat melting curve of bridgmanite observed by Heinz and Jeanloz (1987) and Knittle and Jeanloz (1989). The melting curves

calculated based on bulk modulus at high temperatures are in good agreement with (Zerr and Boehler, 1993) from 24 GPa to 60 GPa. At lower temperatures (Shukla and Wentzcovitch, 2016) and/or higher Fe^{3+} content (Hsu et al., 2011), a small decrease in K_T across the spin transition is apparent as observed for ferropericlase, however, not directly applicable for comparison to extant experimental data (Fig. S2a,c).

To sum up, Lindemann's Law predicts a relatively large melting slope of bridgmanite with ~10 mol% iron at 25 GPa and supports the melting curves reported by (Zerr and Boehler, 1993). Additionally, although the melting temperature depression caused by the spin transition of iron is negligible for bridgmanite with small amounts of Fe^{3+} in the B site (Hummer and Fei, 2012), melting temperature depression may be substantial when the B site Fe^{3+} content is greater such that the spin transition has a more pronounced softening on the thermoelastic properties.

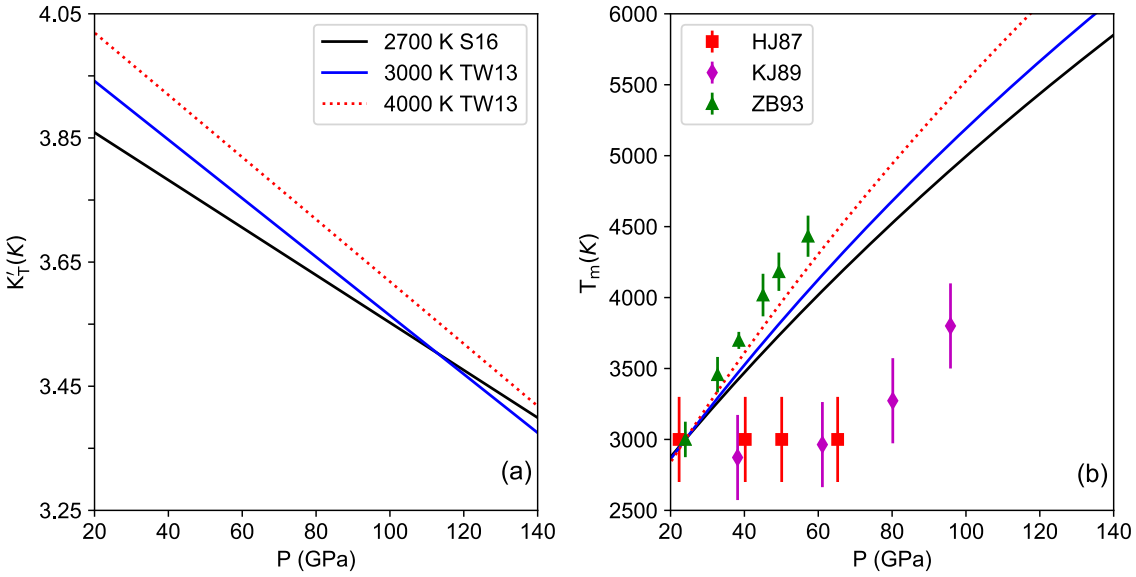

FIGURE 2. Comparison of the melting curves predicted by Lindemann's Law for bridgmanite. **(a)** The evolution of K_T' with pressure across the spin transition for

258 $(Mg_{0.95}Fe^{3+}_{0.05})(Si_{0.95}Fe^{3+}_{0.05})O_3$ at 2700 K (black solid, S16) by (Shukla et al., 2016a) and
259 for $(Mg_{0.9375}Fe^{3+}_{0.0625})(Si_{0.9375}Fe^{3+}_{0.0625})O_3$ at 3000 and 4000 K (blue solid and red dotted)
260 by (Tsuchiya and Wang, 2013). **(b)** Solidus curves of bridgmanite predicted by
261 Lindemann's Law with reference point at 24 GPa and 3000 K according to experiments by
262 (Zerr and Boehler, 1993). Previous experimentally determined melting temperatures of
263 bridgmanite are also shown ($(Mg_{0.9}Fe_{0.1})SiO_3$ by HJ87 (Heinz and Jeanloz, 1987) (red
264 squares), $(Mg_{0.88}Fe_{0.12})SiO_3$ by KJ89 (Knittle and Jeanloz, 1989) (purple diamonds), and
265 $(Mg_{0.88}Fe_{0.12})SiO_3$ by ZB93 (Zerr and Boehler, 1993) (green triangles) where the pressures
266 reported already include thermal pressure. See Fig. S2 for and resulting melting
267 temperature curves computed for other compositions and lower temperatures.

268

269 **Thermodynamics of melting depression**

270 Lindemann's Law relates the melting temperature depression caused by the
271 electronic spin transition in iron to the decrease of the vibrational frequency of atoms. In
272 this section, we explore the thermodynamic basis of the melting depression caused by the
273 spin transition. We show that the fundamental thermodynamic source for the melting
274 depression and elastic anomaly are inherently connected. We consider a pseudo-binary of
275 isochemical HS and LS (Mg,Fe)O or (Mg,Fe)(Si,Fe)O_3. The Gibbs free energies for the
276 liquid (L) and solid (S) are,

277 $$G^{L,S} = (1 - X_{LS})G^{L,S}_{HS} + X_{LS}G^{L,S}_{LS} + G^{L,S}_{mix}, \quad (4)$$

278 where X_{LS} is the fraction of LS states. Note that for a fixed chemical composition X_{LS} is a
279 function of pressure and temperature. $G^{L,S}_{mix}$ is the free energy of mixing and is given by,

$$G_{mix}^{L,S} = H_{mix}^{L,S} - TS_{mix}^{L,S}, \quad (5)$$

where H_{mix} (S_{mix}) is the enthalpy (entropy) of mixing. The volume of a mixture is

$$V = \left(\frac{\partial G}{\partial P}\right)_T = \left(\frac{\partial G}{\partial P}\right)_{T,X_{LS}} + \left(\frac{\partial G}{\partial X_{LS}}\right)_{T,P}\left(\frac{\partial X_{LS}}{\partial P}\right)_T,$$

Since $\left(\frac{\partial G}{\partial X_{LS}}\right)_{T,P} = 0$ at equilibrium (Wu *et al*., 2009), the V is further expressed as

$$V = (1 - X_{LS})V_{HS} + X_{LS}V_{LS} + V^E \quad (6)$$

where $V_{HS/LS}$ is the volume of the HS (LS) endmember and $V^E = (\partial G_{mix}/\partial P)_{T,X_{LS}} = (\partial H_{mix}/\partial P)_{T,X_{LS}}$. The isothermal bulk modulus of a mixture with a fixed chemical composition but varying X_{LS} may be expressed as,

$$\frac{1}{K_T} = -\frac{1}{V}\left(\frac{\partial V}{\partial P}\right)_T = \frac{1}{V}\left((1 - X_{LS})\frac{V_{HS}}{K_{T,HS}} + X_{LS}\frac{V_{LS}}{K_{T,LS}} - \left(\frac{\partial V^E}{\partial P}\right)_T - (V_{LS} - V_{HS})\left(\frac{\partial X_{LS}}{\partial P}\right)_T\right), \quad (7)$$

where $K_{T,HS/LS}$ is the bulk modulus of the HS (LS) endmember. The bulk modulus depression for ferropericlase and bridgmanite upon spin transition derives from the condition,

$$\left(\frac{\partial V^E}{\partial P}\right)_T + (V_{LS} - V_{HS})\left(\frac{\partial X_{LS}}{\partial P}\right)_T < 0, \quad (8)$$

The second term, $(V_{LS} - V_{HS})(\partial X_{LS}/\partial P)_T$ is always negative since $V_{LS} < V_{HS}$ and $(\partial X_{LS}/\partial P)_T > 0$ upon spin transition. For solids, the mixing of HS and LS $(Mg_{1-x},Fe_x)O$ has long been assumed to be ideal (Tsuchiya et al., 2006; Wentzcovitch et al., 2009). In this case, the $H_{mix} = 0$ and the condition (8) is trivial. Yet, recent first-principles computations found the mixing of HS and LS $(Mg_{1-x},Fe_x)O$ is non-ideal with $H_{mix} < 0$ and at least for 0 K $\left(\frac{\partial V^E}{\partial P}\right)_T > 0$ (Holmström and Stixrude, 2015). Eq. 8 requires that

299 $(\partial^2 H_{mix}/\partial P^2)_T < (V_{HS} - V_{LS})(\partial X_{LS}/\partial P)_T$. Nevertheless, the observed softening of
300 ferropericlase, bridgmanite, and some other transition metal bearing minerals (Liu et al.,
301 2014; Wu et al., 2016) suggests that Eq. 8 is met for these systems.

302 Both theoretical and experimental studies focus on the elastic anomaly due to spin
303 transition of iron in the solids. For the liquid system with spin transition of iron,
304 $(V_{LS} - V_{HS})(\partial X_{LS}/\partial P)_T$<0 still holds. Whether or not this elastic depression still exists
305 hinges on the relative largeness of the two terms in Eq. 8 and is unclear so far.

306 In contrast to the elastic anomaly where the thermodynamic parameters of a single
307 phase (either solid or liquid) are involved, the melting depression involves the
308 thermodynamics of both phases. To simplify the consideration here, we use the regular
309 solution model to describe both liquid and solid phases,

310 $$H_{mix}^{L,S} = a^{L,S} X_{HS}^{L,S} X_{LS}^{L,S}, \quad (9)$$

311 where $a^{L,S}$ is the Margules parameter and $X_{HS}^{L,S}$ ($X_{LS}^{L,S}$) is the high (low) spin component
312 fraction. At least for the solid, this simple regular solution model is justified as first-
313 principles simulations yield $H_{mix}^{L,S}$ that are nearly symmetric parabolas (Holmström and
314 Stixrude, 2015).

315 Melting depression discussed in the previous sections means that a portion of the
316 solidus of the HS-LS binary is lower than the melting temperatures of both end-members.
317 Therefore, we focus on the effects of spin states on shape of the phase loops. We first
318 consider the melting depression in the binary system, FeO(HS)-FeO(LS) and the ternary
319 FeO(HS)-FeO(LS)-MgO system.

320

This is a preprint, the final version is subject to change, of the American Mineralogist (MSA)
Cite as Authors (Year) Title. American Mineralogist, in press.
DOI: https://doi.org/10.2138/am-2019-6948

Melting temperature depression in FeO(HS)-FeO(LS) binary system

An example of the G_{mix}-X curves (free energy of mixing-composition) for liquid and solid FeO phases at T_1 is shown in Fig 3a. The common tangent of liquid and solid G-X curves dictates the liquid and solid composition in equilibrium at T_1. The point where these two G-X curves cross yields a midrib curve which necessarily lies within the two-phase field in Fig. 3b (Dehoff, 2006).

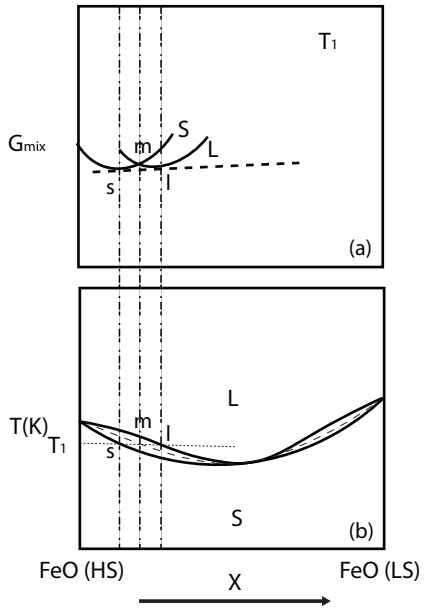

FIGURE 3. Illustration of the construction of the mid-rib curve. **(a)** Free energy of mixing for solid (S) and liquid (L) FeO as a function of spin states (HS, high-spin; LS, low-spin) at T_1 and a fixed pressure. The S, L curves are meant to be schematic and should not be extrapolated beyond the composition range considered here. **(b)** A schematic of the isobaric binary phase diagram of FeO (HS) and FeO (LS). The midrib curve (thin dashed curve) lies in between the liquidus and solidus. The three vertical dotted-dashed lines intersect with the liquidus, midrib, and solidus curves at points *l*, *m*, and *s* respectively. The

common tangent intersects the G_{mix} of liquid and solid at point *l* and *s,* respectively. The G_{mix} of liquid and solid intersect at point *m*.

The midrib curve T_{mid} (X) is defined as,

$$G_{mix}^{S} = G_{mix}^{L}, \tag{10}$$

Note that G_{mix}^{S} and G_{mix}^{L} should have the same references states. Here we define the reference states for both endmembers as solid state. Therefore, for a regular solution model, the Eq. 5 can be further expanded as,

$$G_{mix}^{S} = a^{S} X_{HS}^{S} X_{LS}^{S} + RT\left(X_{HS}^{S}\ln X_{HS}^{S} + X_{LS}^{S}\ln X_{LS}^{S}\right)$$
$$G_{mix}^{L} = a^{L} X_{HS}^{L} X_{LS}^{L} + RT(X_{HS}^{L}\ln X_{HS}^{L} + X_{LS}^{L}\ln X_{LS}^{L}) + X_{HS}^{L}\Delta G_{HS}^{0S\to L} + X_{LS}^{L}\Delta G_{LS}^{0S\to L} \tag{11}$$

where $\Delta G_{HS/LS}^{0S\to L}$is the free energy change during melting for pure HS/LS endmembers and may be expressed as,

$$\Delta G_{HS/LS}^{0S\to L} = \Delta S_{HS/LS}(\Delta T_{m,HS/LS} - T) = (S_{HS/LS}^{L} - S_{HS/LS}^{S})(T_{m,HS/LS} - T), \tag{12}$$

where $\Delta S_{HS/LS}$is the entropy of melting. For midrib curve, $X_{LS}^{S} = X_{LS}^{L} = X$ and $X_{HS}^{S} = X_{HS}^{L} = 1 - X$. Combining this relation with Eqs. 10, 11, and 12 and solving for T_{mid},

$$T_{mid} = \frac{(a^{L}-a^{S})X(1-X)+(1-X)T_{m,HS}\Delta S_{HS}+XT_{m,LS}\Delta S_{LS}}{(1-X)\Delta S_{HS}+X\Delta S_{LS}}, \tag{13}$$

The slope of midrib curve is

$$\frac{dT_{mid}}{dX} = (\Delta S_{HS} - \Delta S_{LS})[(1-X)T_{m,HS}\Delta S_{HS} + XT_{m,LS}\Delta S_{HS} + (X - X^{2})(a^{L} - a^{S})]$$
$$\frac{+(-X\Delta S_{HS} + X\Delta S_{LS} + \Delta S_{HS})[-T_{m,HS}\Delta S_{HS} + T_{m,LS}\Delta S_{LS} + (1-2X)(a^{L} - a^{S})]}{(-X\Delta S_{HS} + X\Delta S_{LS} + \Delta S_{HS})^{2}} \tag{14}$$

352 In order to have melting temperature depression, it is necessary to have a minimum
353 point in the phase loops and consequently in the midrib curve as well (Fig. 3a).
354 Mathematically, it requires that

355 $$\left.\frac{dT_{mid}}{dX}\right|_{X=0} = \frac{(a^L - a^S) - (T_{m,HS} - T_{m,LS})\Delta S_{LS}}{\Delta S_{HS}} < 0 \quad (15)$$

356 and

357 $$\left.\frac{dT_{mid}}{dX}\right|_{X=1} = \frac{-(a^L - a^S) - (T_{m,HS} - T_{m,LS})\Delta S_{HS}}{\Delta S_{LS}} > 0 \quad (16)$$

358 Eqs. 15 and 16 require that

359 $$(a^L - a^S) < (T_{m,HS} - T_{m,LS})\Delta S_{LS} \quad (17)$$

360 and

361 $$(a^L - a^S) < (T_{m,LS} - T_{m,HS})\Delta S_{HS} \quad (18)$$

362 respectively. Because $\Delta S_{HS/LS} > 0$, conditions (17) and (18) imply that a^L should be smaller
363 than a^S in order to induce the melting temperature depression.

364 **Melting temperature depression in FeO(HS)-FeO(LS)-MgO ternary system**

365 The ternary system of FeO(HS), FeO(LS), and MgO is composed of three binary
366 solid solutions, i.e., FeO(HS)-FeO(LS), FeO(HS)-MgO, and FeO(LS)-MgO. The solidus
367 and liquids surfaces divide the parameter space into three regimes, i.e., pure liquid (above
368 the liquidus surface) and pure solid (below the solidus surface), and the two-phase field

where liquid and solid can coexist (Fig. 4). The midrib surface is sandwiched by the solidus and liquidus surfaces (Fig. 4). If the electronic spin crossover causes the melting temperature anomalously depressed, the midrib surface, $T_{\mathrm{mid}}(X_{\mathrm{LS}}, X_{\mathrm{MgO}})$ must obey

$$\left.\frac{dT_{mid}}{dX}\right|_{X_{LS}=0, X_{MgO}=\text{constant}} < 0 \tag{19}$$

and

$$\left.\frac{dT_{mid}}{dX}\right|_{X_{LS}=1, X_{MgO}=\text{constant}} > 0 \tag{20}$$

Similar to the binary system, we first derive the expression for midrib surface. As we focus on the effects of spin states on the melting temperatures, only the enthalpy of mixing for FeO(HS)-FeO(LS) is considered to be non-zero for simplicity. The free energies of mixing for solid and liquid are rewritten as (Mukhopadhyay et al., 1993)

$$\begin{aligned} G^S_{mix} &= a^S X^S_{HS} X^S_{LS} + RT(X^S_{HS}\ln X^S_{HS} + X^S_{LS}\ln X^S_{LS} + X^S_{MgO}\ln X^S_{MgO}) \\ G^L_{mix} &= a^L X^L_{HS} X^L_{LS} + RT(X^L_{HS}\ln X^L_{HS} + X^L_{LS}\ln X^L_{LS} + X^L_{MgO}\ln X^L_{MgO}) \\ &\quad + X^L_{HS}\Delta G^{0S->L}_{HS} + X^L_{LS}\Delta G^{0S->L}_{LS} + X^L_{MgO}\Delta G^{0S->L}_{MgO} \end{aligned} \tag{21}$$

For a midrib surface at fixed MgO content, the midrib surface degenerates into a midrib curve. The points of this midrib curve require $X^S_{LS} = X^L_{LS} = X$, $X^S_{MgO} = X^L_{MgO} = c$, and $X^S_{HS} = X^L_{HS} = 1 - X - c$. Applying these conditions to Eq. 21, we solve for the midrib curve at constant MgO content and further differentiate it with respect to spin states (X). The results are,

This is a preprint, the final version is subject to change, of the American Mineralogist (MSA)
Cite as Authors (Year) Title. American Mineralogist, in press.
DOI: https://doi.org/10.2138/am-2019-6948

$$\left.\frac{dT_{mid}}{dX}\right|_{X=0,X_{MgO}=c} = (\Delta S_{HS}-\Delta S_{LS})[(1-c)T_{m,HS}\Delta S_{HS}+cT_{m,MgO}\Delta S_{MgO}] + [(1-c)\Delta S_{HS}+c\Delta S_{MgO}][-T_{m,HS}\Delta S_{HS}+T_{m,LS}\Delta S_{LS}+(1-c)(a^L-a^S)] \Big/ (-c\Delta S_{HS}+\Delta S_{HS}+c\Delta S_{MgO})^2 < 0 \quad (22)$$

and

$$\left.\frac{dT_{mid}}{dX}\right|_{X=1,X_{MgO}=c} = (\Delta S_{HS}-\Delta S_{LS})[-cT_{m,HS}\Delta S_{HS}+T_{m,LS}\Delta S_{LS}+cT_{m,MgO}\Delta S_{MgO}-(a^L-a^S)c] + (-c\Delta S_{HS}+\Delta S_{LS}+c\Delta S_{MgO})[-T_{m,HS}\Delta S_{HS}+T_{m,LS}\Delta S_{LS}-(a^L-a^S)(c+1)] \Big/ (-c\Delta S_{HS}+\Delta S_{LS}+c\Delta S_{MgO})^2 > 0 \quad (23)$$

As expected, Eqs. 22 and 23 degenerate to Eqs 15 and 16 respectively at c=0. For 0<c<1, Eqs. 22 and 23 do not give a simple relation between $a^L - a^S$ and other thermodynamic parameters. Nevertheless, some general trends could be resolved if one assumes FeO of pure high and low spin states have identical entropy of melting (i.e, $\Delta S_{HS} = \Delta S_{LS} = \Delta S$) given that the chemical species of these two systems are identical. Above inequalities yield,

$$a^L - a^S < \frac{(T_{m,HS}-T_{m,LS})\Delta S}{1-c} \quad (24)$$

and

$$a^L - a^S < \frac{(T_{m,LS}-T_{m,HS})\Delta S}{c+1}, \quad (25)$$

where 0<c<1. Similar to Eqs. 17, 18, the right hand side of either Eq. 24 or Eq. 25 is negative, which requires that the Margules parameter of liquid smaller than the Margules

This is a preprint, the final version is subject to change, of the American Mineralogist (MSA)
Cite as Authors (Year) Title. American Mineralogist, in press.
DOI: https://doi.org/10.2138/am-2019-6948

399 parameter of solid.

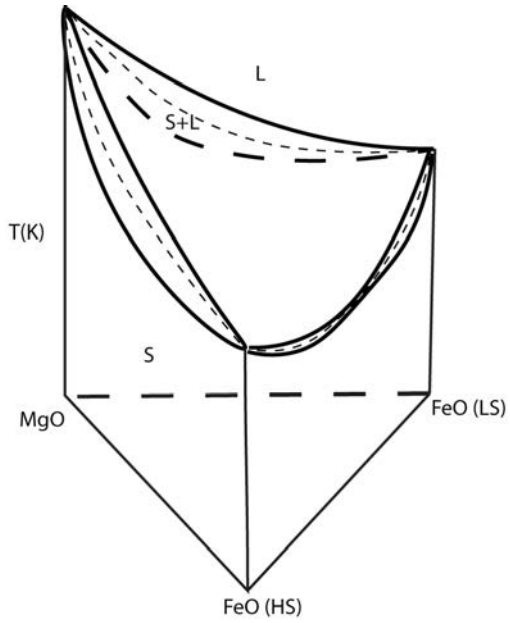

400

401 **FIGURE 4.** Schematic of isobaric MgO-FeO(HS)-FeO(LS) ternary phase diagram. The
402 midrib surface (thin dashed curve) is located within the two-phase field where liquid (L)
403 and solid (S) coexist.

404 The microscopic meaning of Eqs. 17, 18, 24, and 25 may be described as follows.
405 Margules parameters describe the interaction of the endmember components. Theoretical
406 computations have demonstrated that both Margules parameters a^L and a^S for the liquid
407 and solid, respectively are negative ($H_{mix}^{L,S}$ <0) for (Mg,Fe)O at the pressure and temperature
408 conditions where the spin transition of Fe^{2+} is predicted ($G_{mix}^{L,S}$ <0), indicating that for both
409 liquid and solid (Mg,Fe)O, HS and LS components tend to form a random mixture
410 (Holmström and Stixrude, 2015; Holmstrom and Stixrude, 2016). Furthermore, Eqs. 17,
411 18, 24, and 25 demonstrate that the melting depression experimentally observed for
412 (Mg,Fe)O and predicted by Lindemann's Law for (Mg,Fe)O and B-site Fe^{3+} bearing

413 $(Mg,Fe)SiO_3$ requires the tendency of forming a random mixture in the liquid phase is
414 stronger than that in the solid phase.

415 Mathematically, the conditions for melting depression (Eqs. 17, 18, 24, 25) and
416 elastic softening (Eq. 8) have similar forms and both are the inequality between $H_{mix}^{L,S}$ and
417 HS/LS endmember properties. This similarity demonstrates that the fundamental source
418 for melting depression and for elastic softening are intimately related, although it is still
419 too early to draw the causality between Eqs. 8 and 17, 18, 24, 25 without a good
420 understanding of the H_{mix}^{L}.

421

422 **Implications**

423 We employed Lindemann's Law to confirm the experimentally determined melting
424 temperature depression for Earth-relevant compositions of (Mg,Fe)O ferropericlase across
425 the spin transition. We find the elastic softening of ferropericlase caused by the electronic
426 spin transition is intimately related to the observed melting depression through
427 Lindemann's Law. In contrast, for Earth-relevant compositions of $(Mg,Fe)SiO_3$
428 bridgmanite, Lindemann's Law predicts melting depression would be negligibly small
429 even if the B site Fe^{3+} transitions from the HS to LS state.

430 In addition to the semi-empirical Lindemann's law, a thermodynamic reasoning has
431 been presented to demonstrate the possible connection between the fundamental sources
432 for elastic softening and melting depression. We found that the enthalpy of mixing plays a
433 critical role for both phenomena. Specifically, for a mixture of HS and LS, the zeroth
434 derivative of H_{mix} governs the melting temperature depression (Eqs. 17, 18, 24, and 25);

435 the first derivative controls the extra volume depression (Eq. 6); the second derivative
436 dictates the depression of bulk modulus (Eq. 8). It is interesting to note that at least for
437 (Mg,Fe)O, the zeroth, first, and second derivatives of H_{mix} satisfy the inequalities to
438 manifest the depression of melting temperature, volume, and bulk modulus. Whether this
439 is merely a coincidence or a universal phenomenon for the spin transition of iron remains
440 to be tested.

441 It is noted that apart from (Mg,Fe)O ferropericlase, melting temperature depression
442 has also been observed for some alkali metals (e.g., Na, Li, K, Cs, Rb) (e.g., Young, 1991;
443 Gregoryanz et al., 2005; Raty et al., 2007). Interestingly, these metals also exhibit
444 thermoelastic anomalies (e.g., Martinez-Canales and Bergara, 2008). The spin-transition
445 induced melting temperature depression for lower mantle minerals and observed melting
446 temperature depression for alkali metals may share some fundamental similarities and
447 await future confirmation.

448 While melting depression of ferropericlase and bridgmanite is interesting in its own
449 right, melting depression may affect Earth's overall thermochemical evolution. First,
450 melting temperature is a fundamental material property. As demonstrated above, the scale
451 of melting temperature depression for ferropericlase and bridgmanite of Earth-relevant
452 composition is relatively small as compared to the present geotherm and consequently the
453 depressed melting curves do not intersect with the present geotherm. However, during the
454 crystallization of the magma ocean in an early Earth, the melting depression may have
455 caused the formation of a partial melt layer sandwiched between solid layers within the
456 deep Earth because the crystallization temperatures of especially ferropericlase may be
457 largely depressed at similar depths. This may have some interesting feedback to the

458 evolution of the primordial mantle. Second, melting temperature can be related to other
459 material properties. For example, transport properties (e.g., self-diffusion coefficient and
460 viscosity) may be related to melting temperature through homologous temperature scaling
461 (Deng and Lee, 2017). The melting depression of ferropericlase and bridgmanite upon the
462 spin transition of iron may indicate that these minerals become less viscous (Wentzcovitch
463 et al., 2009; Ammann et al., 2011), which may further influence the mantle convection.

464

465 **Acknowledgments:** We thank Raymond Jeanloz, associate editor Sergio Speziale, and the
466 two anonymous reviewers for very useful comments and suggestions that improved the
467 manuscript. This work was supported by NSF (EAR-1321956, EAR-1551348).

468 **Reference**

469 Ammann, M.W., Brodholt, J.P., and Dobson, D.P. (2011) Ferrous iron diffusion in ferro-
470 periclase across the spin transition. Earth and Planetary Science Letters, 302(3),
471 393-402.

472 Anderson, O.L. (1995) Equations of State of Solids for Geophysics and Ceramic Science.
473 Oxford University Press.

474 -. (1998) Thermoelastic properties of $MgSiO_3$ perovskite using the Debye approach.
475 American Mineralogist, 83(1-2), 23-35.

476 Anderson, O.L., and Hama, J. (1999) Shifts in thermal expansivity with Fe content for
477 solid solutions of $MgSiO_3$-$FeSiO_3$ with the perovskite structure. American
478 Mineralogist, 84(3), 221-225.

479 Badro, J., Fiquet, G., Guyot, F., Rueff, J.P., Struzhkin, V.V., Vanko, G., and Monaco, G.
480 (2003) Iron partitioning in Earth's mantle: Toward a deep lower mantle
481 discontinuity. Science, 300(5620), 789-791.

482 Catalli, K., Shim, S.-H., Prakapenka, V.B., Zhao, J., Sturhahn, W., Chow, P., Xiao, Y.,
483 Liu, H., Cynn, H., and Evans, W.J. (2010) Spin state of ferric iron in $MgSiO_3$
484 perovskite and its effect on elastic properties. Earth and Planetary Science Letters,
485 289(1), 68-75.

Crowhurst, J.C., Brown, J.M., Goncharov, A.F., and Jacobsen, S.D. (2008) Elasticity of (Mg,Fe)O Through the Spin Transition of Iron in the Lower Mantle. Science, 319(5862), 451-453.

Dehoff, R. (2006) Thermodynamics in Materials Science. CRC/Taylor & Francis, Boca Raton.

Deng, J., Du, Z., Benedetti, L.R., and Lee, K.K.M. (2017) The influence of wavelength-dependent absorption and temperature gradients on temperature determination in laser-heated diamond-anvil cells. Journal of Applied Physics, 121(2), 025901.

Deng, J., and Lee, K.K.M. (2017) Viscosity jump in the lower mantle inferred from melting curves of ferropericlase. Nature Communications, 8(1), 1997.

Deng, J., Miyazaki, Y., and Lee, K.K.M. (2019) Implications for the melting phase relations in the MgO-FeO system at core-mantle boundary conditions. Journal of Geophysical Research: Solid Earth, 124.

Du, Z., and Lee, K.K.M. (2014) High-pressure melting of MgO from (Mg,Fe)O solid solutions. Geophysical Research Letters, 41(22), 8061-8066.

Fiquet, G., Andrault, D., Itié, J.P., Gillet, P., and Richet, P. (1996) X-ray diffraction of periclase in a laser-heated diamond-anvil cell. Physics of the Earth and Planetary Interiors, 95(1), 1-17.

Fischer, R.A., and Campbell, A.J. (2010) High-pressure melting of wüstite. American Mineralogist, 95(10), 1473-1477.

Ghosh, D.B., and Karki, B.B. (2016) Solid-liquid density and spin crossovers in (Mg, Fe)O system at deep mantle conditions. Scientific Reports, 6, 37269.

Gilvarry, J.J. (1956a) Equation of the Fusion Curve. Physical Review, 102(2), 325-331.

-. (1956b) The Lindemann and Gruneisen Laws. Physical Review, 102(2), 308-316.

Glazyrin, K., Miyajima, N., Smith, J.S., and Lee, K.K.M. (2016) Compression of a multiphase mantle assemblage: Effects of undesirable stress and stress annealing on the iron spin state crossover in ferropericlase. Journal of Geophysical Research: Solid Earth, 121(5), 2015JB012321.

Gregoryanz, E., Degtyareva, O., Somayazulu, M., Hemley, R.J., and Mao, H.K. (2005) Melting of dense sodium. Physical Review Letters, 94(18).

Heinz, D.L., and Jeanloz, R. (1987) Measurement of the melting curve of Mg0.9Fe0.1SiO3 at lower mantle conditions and its geophysical implications. Journal of Geophysical Research: Solid Earth, 92(B11), 11437-11444.

519 Holmstrom, E., and Stixrude, L. (2016) Spin crossover in liquid (Mg,Fe)O at extreme
520 conditions. Physical Review B, 93(19), 195142.

521 Holmström, E., and Stixrude, L. (2015) Spin Crossover in Ferropericlase from First-
522 Principles Molecular Dynamics. Physical Review Letters, 114(11), 117202.

523 Hsu, H., Blaha, P., Cococcioni, M., and Wentzcovitch, R.M. (2011) Spin-State Crossover
524 and Hyperfine Interactions of Ferric Iron in $MgSiO_3$ Perovskite. Physical Review
525 Letters, 106(11), 118501.

526 Hummer, D.R., and Fei, Y. (2012) Synthesis and crystal chemistry of Fe3+-bearing
527 (Mg,Fe3+)(Si,Fe3+)O3 perovskite. American Mineralogist, 97(11-12), 1915-
528 1921.

529 Knittle, E., and Jeanloz, R. (1989) Melting curve of (Mg,Fe)SiO_3 perovskite to 96 GPa:
530 Evidence for a structural transition in lower mantle melts. Geophysical Research
531 Letters, 16(5), 421-424.

532 Kupenko, I., McCammon, C., Sinmyo, R., Cerantola, V., Potapkin, V., Chumakov, A.I.,
533 Kantor, A., Ruffer, R., and Dubrovinsky, L. (2015) Oxidation state of the lower
534 mantle: In situ observations of the iron electronic configuration in bridgmanite at
535 extreme conditions. Earth and Planetary Science Letters, 423, 78-86.

536 Lawson, A. (2009) Physics of the Lindemann melting rule. 1757-1770 p.

537 Lee, K.K.M., O'Neill, B., Panero, W.R., Shim, S.-H., Benedetti, L.R., and Jeanloz, R.
538 (2004) Equations of state of the high-pressure phases of a natural peridotite and
539 implications for the Earth's lower mantle. Earth and Planetary Science Letters,
540 223(3), 381-393.

541 Lin, J.-F., Mao, Z., Yang, J., Liu, J., Xiao, Y., Chow, P., and Okuchi, T. (2016) High-spin
542 Fe^{2+} and Fe^{3+} in single-crystal aluminous bridgmanite in the lower mantle.
543 Geophysical Research Letters, 43(13), 6952-6959.

544 Lin, J.-F., Speziale, S., Mao, Z., and Marquardt, H. (2013) Effects of the electronic spin
545 transitions of iron in lower mantle minerals: implications for deep mantle
546 geophysics and geochemistry. Reviews of Geophysics, 51(2), 244-275.

547 Lin, J.-F., Vankó, G., Jacobsen, S.D., Iota, V., Struzhkin, V.V., Prakapenka, V.B.,
548 Kuznetsov, A., and Yoo, C.-S. (2007) Spin Transition Zone in Earth's Lower
549 Mantle. Science, 317(5845), 1740-1743.

550 Lindemann, F.A. (1910) über die Berechnung Molecular Eigenfrequnzen. Physikalische
551 Zeitschrift, 11, 609-612.

552 Liu, J., Dorfman, S.M., Zhu, F., Li, J., Wang, Y., Zhang, D., Xiao, Y., Bi, W., and Alp,
553 E.E. (2018) Valence and spin states of iron are invisible in Earth’s lower mantle.
554 Nature Communications, 9(1), 1284.

555 Liu, J., Lin, J.-F., Mao, Z., and Prakapenka, V.B. (2014) Thermal equation of state and
556 spin transition of magnesiosiderite at high pressure and temperature. American
557 Mineralogist, 99(1), 84-93.

558 Mao, Z., Lin, J.F., Liu, J., and Prakapenka, V.B. (2011) Thermal equation of state of
559 lower‐mantle ferropericlase across the spin crossover. Geophysical Research
560 Letters, 38(23).

561 Marquardt, H., Buchen, J., Mendez, A.S.J., Kurnosov, A., Wendt, M., Rothkirch, A.,
562 Pennicard, D., and Liermann, H.-P. (2018) Elastic Softening of $(Mg_{0.8}Fe_{0.2})O$
563 Ferropericlase Across the Iron Spin Crossover Measured at Seismic Frequencies.
564 Geophysical Research Letters, 45(14), 6862–6868.

565 Marquardt, H., Speziale, S., Reichmann, H.J., Frost, D.J., and Schilling, F.R. (2009a)
566 Single-crystal elasticity of $(Mg_{0.9}Fe_{0.1})O$ to 81 GPa. Earth and Planetary Science
567 Letters, 287(3), 345-352.

568 Marquardt, H., Speziale, S., Reichmann, H.J., Frost, D.J., Schilling, F.R., and Garnero,
569 E.J. (2009b) Elastic Shear Anisotropy of Ferropericlase in Earth's Lower Mantle.
570 Science, 324(5924), 224-226.

571 Martinez-Canales, M., and Bergara, A. (2008) Lindemann criterion and the anomalous
572 melting curve of sodium. Journal of Physics and Chemistry of Solids, 69(9),
573 2151-2154.

574 McCammon, C. (1997) Perovskite as a possible sink for ferric iron in the lower mantle.
575 Nature, 387(6634), 694-696.

576 Muir, J.M.R., and Brodholt, J.P. (2016) Ferrous iron partitioning in the lower mantle.
577 Physics of the Earth and Planetary Interiors, 257, 12-17.

578 Mukhopadhyay, B., Basu, S., and Holdaway, M.J. (1993) A discussion of Margules-type
579 formulations for multicomponent solutions with a generalized approach.
580 Geochimica et Cosmochimica Acta, 57(2), 277-283.

581 Ohta, K., Hirose, K., Onoda, S., and Shimizu, K. (2007) The effect of iron spin transition
582 on electrical conductivity of (Mg,Fe)O magnesiowüstite. Proceedings of the Japan
583 Academy. Series B, Physical and Biological Sciences, 83(3), 97-100.

584 Poirier, J.P. (1989) Lindemann law and the melting temperature of perovskites. Physics
585 of the Earth and Planetary Interiors, 54(3), 364-369.

586 Raty, J.-Y., Schwegler, E., and Bonev, S.A. (2007) Electronic and structural transitions in
587 dense liquid sodium. Nature, 449, 448.

588 Saha, S., Bengtson, A., Crispin, K.L., Van Orman, J.A., and Morgan, D. (2011) Effects of
589 spin transition on diffusion of Fe^{2+} in ferropericlase in Earth's lower mantle.
590 Physical Review B, 84(18), 184102.

Shim, S.-H., Grocholski, B., Ye, Y., Alp, E.E., Xu, S., Morgan, D., Meng, Y., and Prakapenka, V.B. (2017) Stability of ferrous-iron-rich bridgmanite under reducing midmantle conditions. Proceedings of the National Academy of Sciences, 114(25), 6468-6473.

Shukla, G., Cococcioni, M., and Wentzcovitch, R.M. (2016a) Thermoelasticity of Fe^{3+}-and Al-bearing bridgmanite: Effects of iron spin crossover. Geophysical Research Letters, 43(11), 5661-5670.

Shukla, G., Cococcioni, M., and Wentzcovitch, R.M. (2016b) Thermoelasticity of Fe^{3+}-and Al-bearing bridgmanite: Effects of iron spin crossover, 43, p. 5661-5670-5661-5670. American Geophysical Union.

Shukla, G., and Wentzcovitch, R.M. (2016) Spin crossover in $(Mg,Fe^{3+})(Si,Fe^{3+})O3$ bridgmanite: Effects of disorder, iron concentration, and temperature. Physics of the Earth and Planetary Interiors, 260, 53-61.

Speziale, S., Zha, C.-S., Duffy, T.S., Hemley, R.J., and Mao, H.-k. (2001) Quasi-hydrostatic compression of magnesium oxide to 52 GPa: Implications for the pressure-volume-temperature equation of state. Journal of Geophysical Research: Solid Earth, 106(B1), 515-528.

Tange, Y., Nishihara, Y., and Tsuchiya, T. (2009) Unified analyses for P‐V‐T equation of state of MgO: A solution for pressure‐scale problems in high P‐T experiments. Journal of Geophysical Research: Solid Earth, 114(B3).

Tsuchiya, T., and Wang, X. (2013) Ab initio investigation on the high-temperature thermodynamic properties of Fe^{3+}-bearing MgSiO3 perovskite. 118(1), 83-91.

Tsuchiya, T., Wentzcovitch, R.M., da Silva, C.R.S., and de Gironcoli, S. (2006) Spin transition in magnesiowustite in earth's lower mantle. Physical Review Letters, 96(19), 198501.

Wallace, D.C. (1991) Melting of elements. Proceedings of the Royal Society of London. Series A: Mathematical and Physical Sciences, 433(1889), 631-661.

Wentzcovitch, R.M., Justo, J.F., Wu, Z., da Silva, C.R.S., Yuen, D.A., and Kohlstedt, D. (2009) Anomalous compressibility of ferropericlase throughout the iron spin cross-over. Proceedings of the National Academy of Sciences, 106(21), 8447-8452.

Wolf, G.H., and Jeanloz, R. (1984) Lindemann Melting Law: Anharmonic correction and test of its validity for minerals. Journal of Geophysical Research: Solid Earth, 89(B9), 7821-7835.

Wu, Y., Wu, X., Lin, J.-F., McCammon, C.A., Xiao, Y., Chow, P., Prakapenka, V.B., Yoshino, T., Zhai, S., and Qin, S. (2016) Spin transition of ferric iron in the NAL

627 phase: Implications for the seismic heterogeneities of subducted slabs in the lower
628 mantle. Earth and Planetary Science Letters, 434, 91-100.

629 Wu, Z., Justo, J.F., da Silva, C.R.S., de Gironcoli, S., and Wentzcovitch, R.M. (2009)
630 Anomalous thermodynamic properties in ferropericlase throughout its spin
631 crossover (vol 80, 014409, 2009). Physical Review B, 80(9).

632 Yang, J., Lin, J.-F., Jacobsen, S.D., Seymour, N.M., Tkachev, S.N., and Prakapenka,
633 V.B. (2016) Elasticity of ferropericlase and seismic heterogeneity in the Earth's
634 lower mantle. Journal of Geophysical Research: Solid Earth, 121(12),
635 2016JB013352.

636 Yang, J., Tong, X.Y., Lin, J.F., Okuchi, T., and Tomioka, N. (2015) Elasticity of
637 Ferropericlase across the Spin Crossover in the Earth's Lower Mantle. Scientific
638 Reports, 5.

639 Young, D.A. (1991) Phase Diagrams of the Elements. University of California Press.

640 Zerr, A., and Boehler, R. (1993) Melting of (Mg,Fe)SiO_3-Perovskite to 625 Kilobars -
641 Indication of a High-Melting Temperature in the Lower Mantle. Science,
642 262(5133), 553-555.

643

644